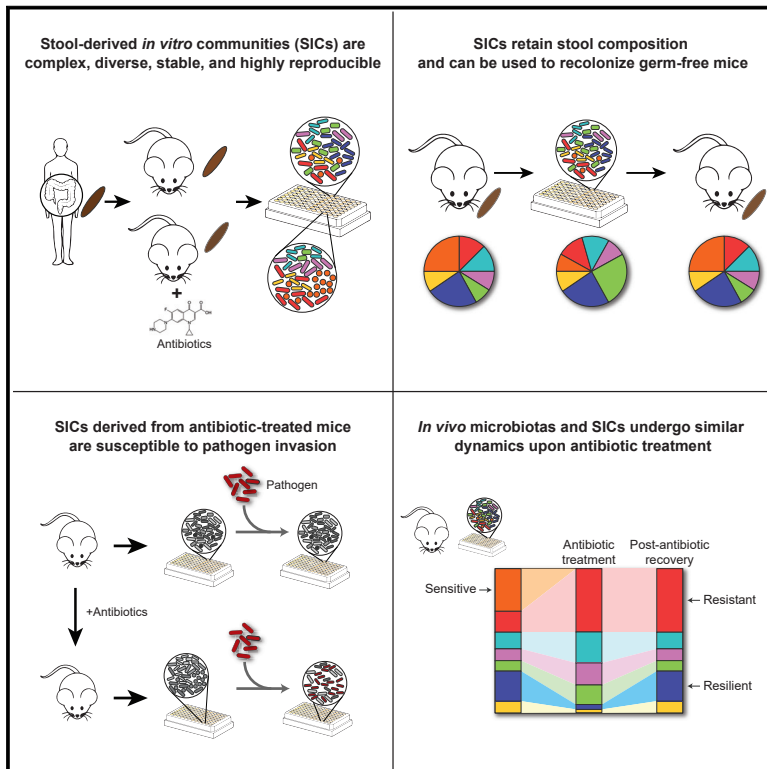# Establishment and characterization of stable, diverse, fecal-derived *in vitro* microbial communities that model the intestinal microbiota

Graphical abstract

Authors

Andrés Aranda-Díaz,
Katharine Michelle Ng,
Tani Thomsen, ..., Joshua E. Elias,
Justin L. Sonnenburg,
Kerwyn Casey Huang

Correspondence

kchuang@stanford.edu

In brief

Aranda-Díaz et al. demonstrate the utility of batch culturing of stool-derived *in vitro* communities (SICs) for low-cost, quantitative, and high-throughput experimentation on gut microbiotas. SICs retain the taxonomical diversity of their fecal origin and recapitulate the microbiota response to pathogen invasion and antibiotic treatment.

Highlights

- Stool-derived *in vitro* communities (SICs) can be phylogenetically complex and reproducible

- Mouse colonization with a SIC establishes near-native microbiota composition and host proteome

- Antibiotic treatment *in vivo* increases susceptibility to *Salmonella* invasion *in vitro*

- Antibiotic treatment *in vitro* mimics compositional changes *in vivo*

CellPress

Establishment and characterization of stable, diverse, fecal-derived *in vitro* microbial communities that model the intestinal microbiota

Andrés Aranda-Díaz,[1] Katharine Michelle Ng,[1] Tani Thomsen,[1] Imperio Real-Ramírez,[1] Dylan Dahan,[2] Susannah Dittmar,[1] Carlos Gutierrez Gonzalez,[3] Taylor Chavez,[1] Kimberly S. Vasquez,[2] Taylor H. Nguyen,[1] Feiqiao Brian Yu,[4] Steven K. Higginbottom,[2] Norma F. Neff,[4] Joshua E. Elias,[4] Justin L. Sonnenburg,[2,4] and Kerwyn Casey Huang[1,2,4,5,*]

[1]Department of Bioengineering, Stanford University, Stanford, CA 94305, USA
[2]Department of Microbiology and Immunology, Stanford University School of Medicine, Stanford, CA 94305, USA
[3]Department of Chemical and Systems Biology, Stanford University School of Medicine, Stanford, CA 94305, USA
[4]Chan Zuckerberg Biohub, San Francisco, CA 94158, USA
[5]Lead contact
*Correspondence: kchuang@stanford.edu
https://doi.org/10.1016/j.chom.2021.12.008

SUMMARY

Efforts to probe the role of the gut microbiota in disease would benefit from a system in which patient-derived bacterial communities can be studied at scale. We addressed this by validating a strategy to propagate phylogenetically complex, diverse, stable, and highly reproducible stool-derived communities *in vitro*. We generated hundreds of *in vitro* communities cultured from diverse stool samples in various media; certain media generally preserved inoculum composition, and inocula from different subjects yielded source-specific community compositions. Upon colonization of germ-free mice, community composition was maintained, and the host proteome resembled the host from which the community was derived. Treatment with ciprofloxacin *in vivo* increased susceptibility to *Salmonella* invasion *in vitro*, and the *in vitro* response to ciprofloxacin was predictive of compositional changes observed *in vivo*, including the resilience and sensitivity of each *Bacteroides* species. These findings demonstrate that stool-derived *in vitro* communities can serve as a powerful system for microbiota research.

INTRODUCTION

The gut microbiota is a diverse community that performs functions important for host physiology (Hooper et al., 2012; Mayer et al., 2014; Sonnenburg and Bäckhed, 2016), and a wide range of environmental perturbations (Kashyap et al., 2013; Schubert et al., 2015; Tropini et al., 2018) lead to changes in community composition and function. Human and animal models have enabled some mechanistic understanding of these responses (Faith et al., 2011; Mark Welch et al., 2017; Reyes et al., 2013; Rezzonico et al., 2011), yet insight into microbiota recovery in even the most well-studied case (antibiotics) is limited. Antibiotics disrupt colonization resistance and lead to pathogen expansion and fecal shedding (Barthel et al., 2003; Stecher et al., 2007) and can dramatically affect host physiology, including changes in adiposity, insulin resistance, and cognitive function (Cho et al., 2012; Cox et al., 2014; Fröhlich et al., 2016; Hwang et al., 2015). Understanding antibiotic effects across microbiotas, doses, and treatment regimens will assist in mitigating these adverse effects.

We recently showed, using mice colonized with human feces, that the microbiota shifts into a new, lower-diversity steady state after ciprofloxacin treatment, although certain taxa displayed a high level of resilience during recovery (Ng et al., 2019). It is unclear to what extent the response of each taxon can be predicted from its behavior in isolation; microbial interactions and drug modification can impact the efficacy of antibiotic treatment (Adamowicz et al., 2018; Aranda-Díaz et al., 2020; de Vos et al., 2017; Nicoloff and Andersson, 2016), which may underlie our current inability to explain individualized responses to fluoroquinolone treatment in humans (Dethlefsen and Relman, 2011), or why some antibiotics negatively impact taxa known to be resistant to the drug *in vitro* (Ivanov et al., 2008). Addressing these questions requires microbiota models that are scalable and high throughput, and in which the magnitude of perturbations can be quantitatively tuned; *in vivo* investigations are limited in these regards.

In vitro co-culturing of collections of isolated species has revealed key interspecies interactions and metabolic roles (de Vos et al., 2017; Gutiérrez and Garrido, 2019; Kehe et al., 2019; Venturelli et al., 2018). However, such synthetic communities generally lack the complexity of gut microbiotas; further, microbes within a host coevolve (Barroso-Batista et al., 2020), which could underlie individualized responses to antibiotics

([Dethlefsen and Relman, 2011](#)). It is also difficult to select which set of species best models the mammalian gut without knowledge of interspecies interactions. Sophisticated continuous-flow culture models ([Macfarlane et al., 1998](#); [Minekus et al., 1999](#)) permit long timescale experimentation and the manipulation of key environmental variables but are also limited in throughput ([Auchtung et al., 2016](#)). Resuspension of stool in liquid media has shown promise for high-throughput analysis of drug metabolism by highly complex communities ([Zimmermann et al., 2019](#)), but the extent to which these approaches recapitulate gut microbiota behaviors is unclear. Passaging of diverse microbiotas from leaf and soil samples in minimal media led to the selection of simple communities whose family-level—but not species-level—compositions were governed by nutrient availability ([Goldford et al., 2018](#)). Whether these findings also apply to human-relevant microbiotas and more complex media is unknown.

Here, we establish that stool-derived *in vitro* communities (SICs) are powerful tools for modeling responses of the gut microbiota to antibiotics *in vivo*. We demonstrate that hundreds of SICs generated from distinct initial inocula in diverse media can be phylogenetically complex and diverse, and stably preserve the composition of the initial inoculum. SIC composition was maintained during colonization of gnotobiotic mice, and the host proteome was mostly reprogrammed in the same manner as the original humanization. SICs derived from the feces of ciprofloxacin-treated mice exhibited increased invasion by the pathogen *Salmonella* Typhimurium *in vitro*, consistent with previously observed decreases in colonization resistance after antibiotic treatment *in vivo*. Ciprofloxacin caused similar compositional changes in SICs and humanized mice, highlighting the utility of SICs for predicting and interpreting the results of *in vivo* experiments in high throughput.

RESULTS

Anaerobic batch culturing of humanized mice feces results in stable and reproducible *in vitro* communities

To generate SICs in a straightforward, scalable, and reproducible manner, we focused on ex-germ-free mice colonized with human feces (humanized mice). These humanized mice facilitate controlled experimental manipulation, enabling comparisons between *in vitro* and *in vivo* behaviors of communities of human commensals. We inoculated humanized mouse fecal samples into various media and repeatedly passaged in anaerobic batch cultures in high throughput ([Figure 1](#)A).

To determine whether SICs reached stable compositions, we performed 16S sequencing on SICs derived from the feces of mice fed a diet deficient in microbiota-accessible carbohydrates (MACs) and grown in the complex medium brain heart infusion (BHI). At the family level, SICs stabilized by the second passage ([Figure 1](#)B) and retained most families from the original feces ([Figure 1](#)C). Of the families present in the inoculum but not in the passaged SIC, most were at low abundance *in vivo* ([Figure 1](#)C), with the exception of the Verrucomicrobiaceae ([Figures 1](#)B and 1C). In turn, the sole family to emerge from undetectable levels was the Enterobacteriaceae ([Figures 1](#)B and 1C), whose members have been associated with dysbiosis. The fraction of amplicon sequence variants (ASVs, a proxy for strains) detect-

able in the fecal sample that were detectable on average beyond the fourth passage was 39.1% ± 2.6% (23/58 ASVs). Of the lost ASVs, their median $\log_{10}$(relative abundance) in the inoculum was lower than that of the retained ASVs (-2.46 and -2.05, respectively; p = 0.006 Wilcoxon test). Furthermore, they constituted 55.1% of the inoculum, of which 38.0% corresponded to *A. muciniphila*, which has been shown to be fastidious ([Tramontano et al., 2018](#)). Lost ASVs were lost early in the culturing experiment, in 1.6 ± 0.7 passages. Of the 37 ASVs lost in at least one replicate, 92% were lost in all three replicates, suggesting that ASV loss was not due to bottleneck effects of dilution during passaging. Thus, even though family-level composition is preserved for families conducive to culturing in these conditions, passaging leads to deterministic decreases to levels below the limit of detection, biased toward species that start at lower abundance.

A previous soil and leaf microbiota passaging study reported that despite convergence at the family level, genus-level composition was highly divergent across technical replicates ([Goldford et al., 2018](#)). In our experiments, family-level dynamics were similar ([Figure S1](#)A), and the relative abundances of ASVs were highly correlated across all replicates ([Figures 1](#)D and [S1](#)B). The fractions of families and genera that were detectable after passaging were higher than the fraction of ASVs that remained detectable (39.1%) and similar to each other (52.9% and 56.0%, respectively), suggesting that loss of a genus often meant the loss of an entire family. Three technical replicates of SICs derived from one mouse contained 50 ASVs at >0.1% (a conservative measure of detectability), and all ASVs present in only one replicate had relative abundance <1%; higher variation in low-abundance ASVs is expected due to counting noise. SIC composition was also maintained in higher-volume culturing ([Figure S1](#)C) and after freezing and thawing ([Figure S1](#)D). Thus, top-down *in vitro* cultivation from fecal samples can deterministically select complex SICs that are stable during passaging for several weeks.

Colonization of gnotobiotic mice with an SIC re-establishes gut microbiota composition and the host proteome

To determine whether and how SIC composition would be altered by colonization of a mammalian host, we introduced an SIC into germ-free mice ([Figure 2](#)A). Family-level abundances were similar to those of the humanized mice from which the SIC was derived ([Figures 2](#)B and [S1](#)E), and the Enterobacteriaceae that were overrepresented *in vitro* receded *in vivo*. To evaluate effects on host physiology, we quantified host and microbial proteins in the feces of humanized mice, germ-free mice, and SIC-colonized mice. Host proteomes of SIC-colonized mice were more similar to humanized mice than germ-free mice, with immunoglobulins upregulated in SIC-colonized mice ([Figures 2](#)C–2E and [S1](#)F). Therefore, re-introduction of SICs into a host largely re-establishes gut microbiota composition and the host proteome.

Initial inoculum composition and nutrient conditions affect SIC composition

To probe the determinants of SIC composition, we inoculated multiple media with a set of fecal samples that varied widely in
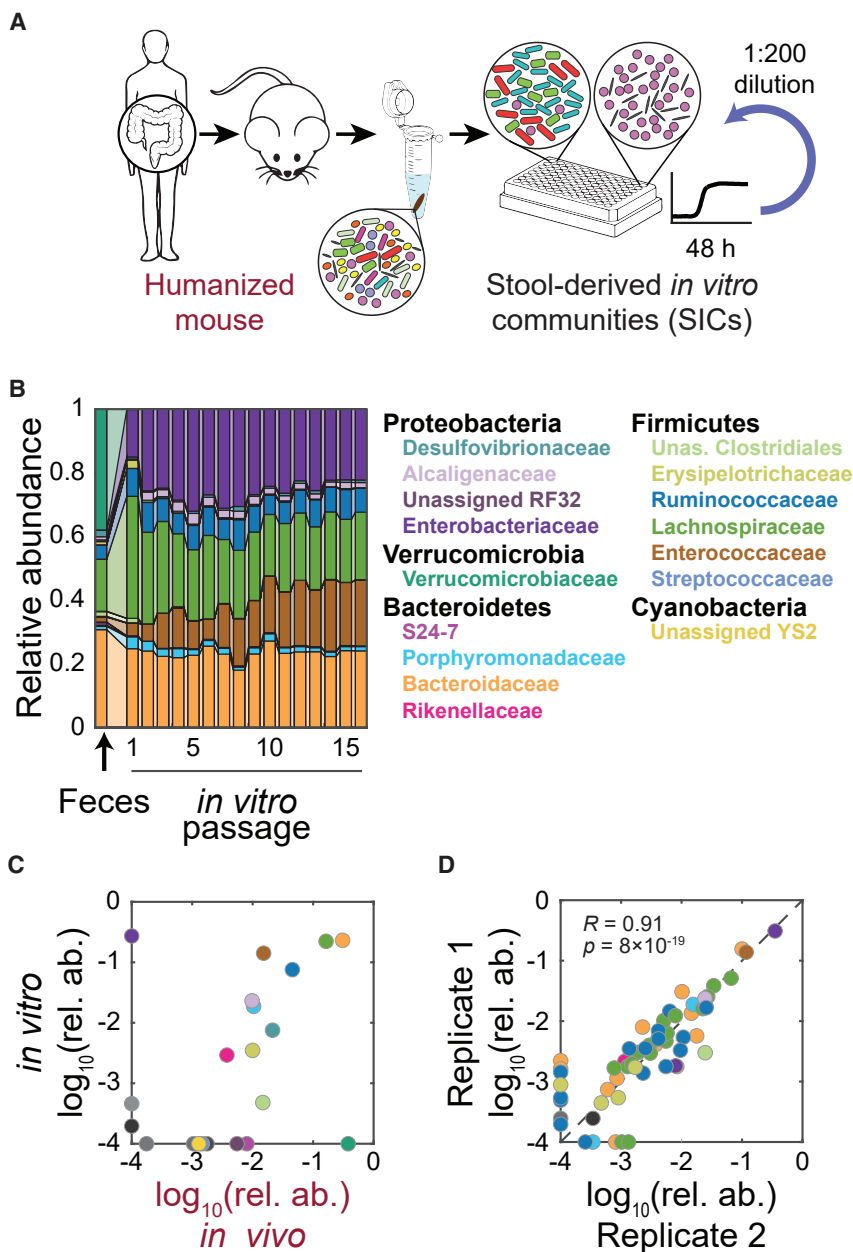
Figure 1. High-throughput cultivation of feces from humanized mice yields stable, complex, and reproducible microbial communities

(A) Experimental setup. Germ-free mice were colonized with feces from a single human donor ("humanized"). Fecal samples from humanized mice were inoculated into anaerobic batch culture and passaged with dilution every 48 h to derive SICs.

(B) *In vitro* passaging produces stable and complex SICs. Family-level compositions of a representative SIC derived from the feces of MD mouse 1 during 16 rounds of *in vitro* passaging in BHI.

(C) *In vitro* passaging can produce an SIC that resembles the fecal inoculum. Family-level relative abundances (mean of passages 4–16) for the SIC in (B) compared with the fecal inoculum from which it originated.

(D) *In vitro*-passaged SICs are highly reproducible. ASV-level relative abundances for two technical replicates of the SIC in (B) after 7 passages. *R* and p were computed using only ASVs present in both samples.

Relative abundances $<10^{-4}$ (in C and D) were set to 10^{-4} for visualization.

to day 5, followed by partial recovery (Figure S2C). Thus, these fecal samples yielded qualitatively different inocula yet with the potential for overlapping strains.

To determine the extent to which the abiotic environment and inoculum dictated steady-state SIC composition, we inoculated the 16 fecal samples into four media (BHI, tryptone-yeast extract-glucose [TYG], Gifu anaerobic medium [GAM], and yeast extract, casitone, and fatty acids [YCFA]) and grew them in technical triplicates for ≥ 7 passages of anaerobic batch culturing. SICs were generally stable and reproducible in BHI and TYG (Figures S3A and S3B); in GAM and YCFA, SICs were prone to fluctuations (Figures S3A–S3C). All BHI SICs were robust to freezing and to growth in higher volumes (Figure S4). In a principal coordinates analysis of 16S

composition yet were composed of a common set of members so that they could be readily compared. We previously discovered that diet and antibiotics have large, distinct, interacting effects on the composition of the microbiota (Ng et al., 2013; Sonnenburg et al., 2016). Thus, we treated mice fed a standard diet (SD) or a MAC-deficient diet (MD) with ciprofloxacin for 5 days. We quantified microbiota composition before treatment (Pre), at the peak of treatment (Peak), during residual treatment (Res), and after (Post) treatment (Figure 3A). As expected, treatment induced distinct microbiotas for the two diets (Figure 3B). Nonetheless, mice generally exhibited reductions in Bacteroidetes and Proteobacteria and expansions in Firmicutes at the peak of treatment (Figures S2A and S2B), and the number of uniquely detected ASVs (richness) dropped steadily from day 1

data of all communities (Figure 3C), the first coordinate was largely determined by the presence or absence of several co-occurring families, including Enterobacteriaceae (Figure S5A). Most of these families were present in pre-treatment inocula and were undetectable in residual treatment (day 5) inocula (Figure S5B), suggesting that the variation is mostly explained by the fecal inocula, not the culture media. Our data approximately clustered according to culture media; BHI and TYG SICs overlapped but were well separated from GAM and even more so from YCFA (Figure 3C). BHI, TYG, and GAM SICs were more similar to their inocula than YCFA SICs when using a weighted approach that accounts for taxonomical relative abundances (Figure 3D). Using presence and absence of taxa as a measure of similarity (thus giving more weight to low-abundance taxa),
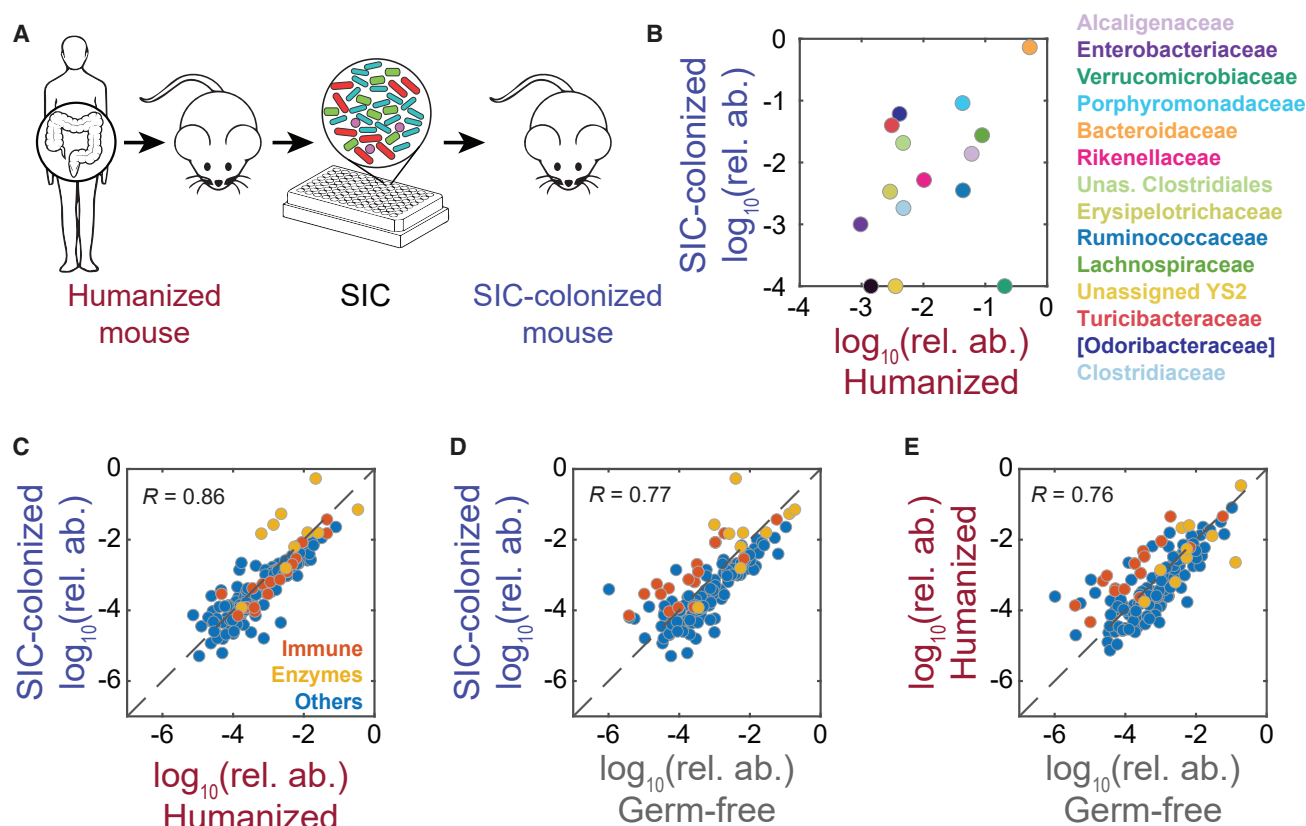
Figure 2. Re-introduction of SICs into a host re-establishes gut microbiota composition and promotes host homeostasis
(A) An SIC generated from a humanized mouse was used to colonize germ-free mice to determine whether SICs can re-establish the original microbiota.
(B) SIC colonization of germ-free mice restored families overrepresented *in vitro* back to levels similar to those in the humanized mice from which the SIC was derived. Comparison of the family-level relative abundances of a humanized mouse fecal inoculum and the mean family-level relative abundance of germ-free mice colonized with an SIC derived from the humanized mouse fecal inoculum (inoculum n = 1, SIC-colonized n = 3). Relative abundances <10^{-4} were set to 10^{-4} for visualization.
(C–E) The host proteomes in humanized and SIC-colonized mice were more highly correlated (C) than either set of mice with germ-free mice (D and E). Immune-related proteins (red) were similarly upregulated in humanized and SIC-colonized mice relative to germ-free mice.

these data suggest that BHI and TYG are reasonable mimics of the conditions that produced the fecal pellet (Figures 3C and S5C–S5E), regardless of inoculating composition. The data also clustered according to the time during antibiotic treatment when the inocula were sampled (Figures 3C and S5C). The direction separating clusters of sampling time was approximately orthogonal to the direction separating SICs by medium (Figures 3C and S5C), indicating that both the availability of taxa in the inoculum and the ability of those taxa to grow in a given medium dictate the composition of SICs.

We computed Pearson correlation coefficients of ASV abundances among pairs of technical replicates for all combinations of inoculum and medium and found that 90% were >0.68 (Figure S3A), with a mean and standard deviation of 0.86 ± 0.22 (n = 192). Across all pairwise comparisons, the mean number of unique ASVs (>0.1% in one replicate and not detectable in the other) was very low (3.0 ± 3.3, n = 384), with a mean log$_{10}$(relative abundance) of −2.24 ± 0.62 (n = 1171), suggesting that many instances of unique ASVs were due to abundances lower than the limit of detection rather than due to stochasticity in passaging. SICs cultured in YCFA had the largest proportion of

replicates with low correlation coefficients (<0.6; Figures S3A and S3B), while every pair of replicates cultured in BHI had a correlation coefficient >0.6 (Figures S3B and S3C). Half of the technical replicates shared members that constituted >99% of the total abundance, while only ~1% had shared members accounting for <5%. In general, the lowest replicability was observed in YCFA and in SICs cultured from inocula with low diversity (Figures S2C and S3A–S3C), suggesting that higher diversity promotes deterministic behavior during passaging. Intriguingly, these findings indicate that SICs are not generally stable in GAM and YCFA, despite the ability of these media to promote the growth of many commensals in isolation (Browne et al., 2016; Rettedal et al., 2014).

SIC richness is highly correlated with that of the fecal sample due to the maintenance of abundant species and within-family replacement

The presence or absence of multiple families dictating the first principal coordinate (Figure S5A), and the observation that this coordinate mainly separated SICs by their inocula (Figure 3C), suggested that SIC richness depends on the richness of the
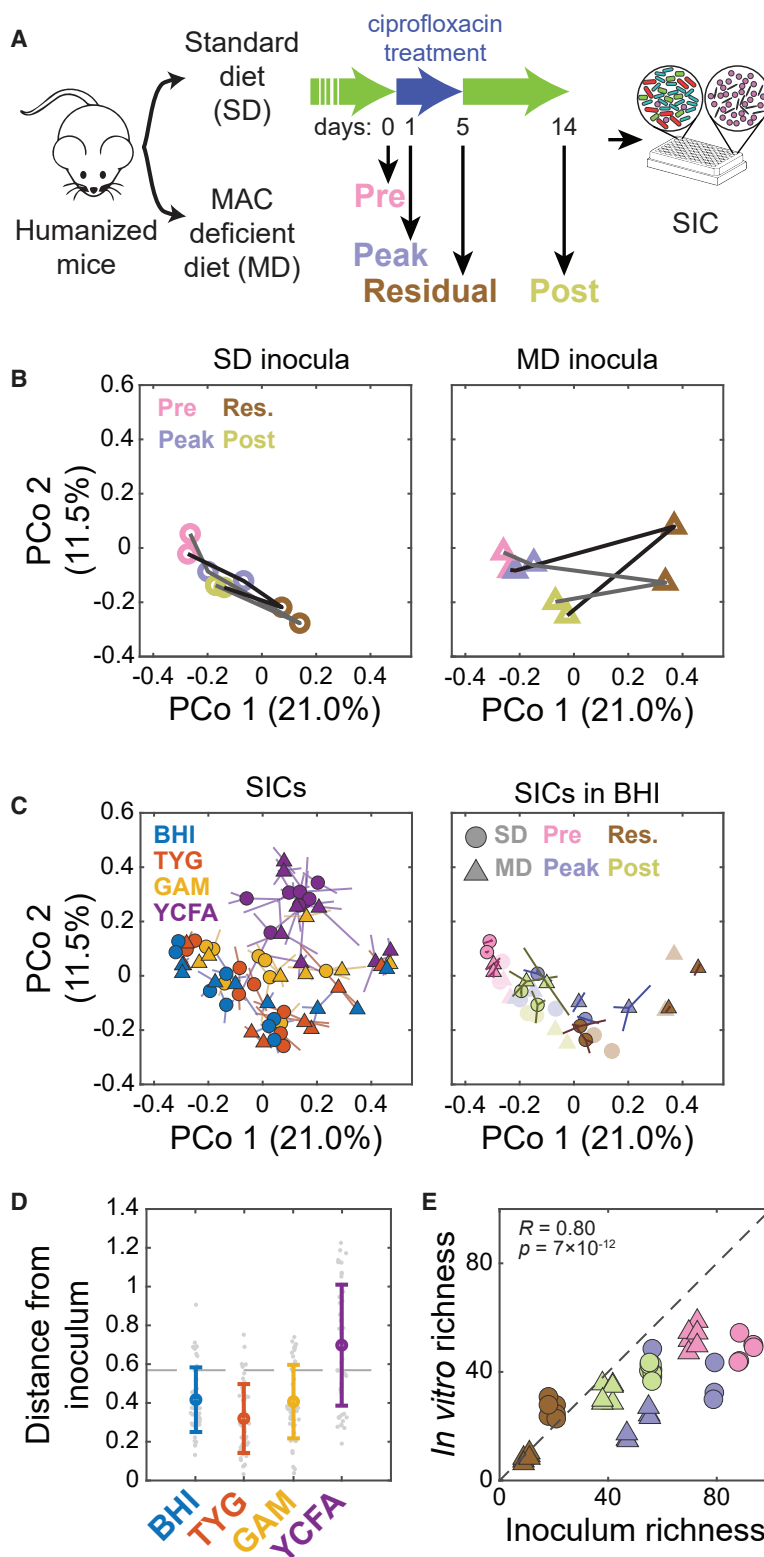
A

Figure 3. High-throughput cultivation of humanized mouse feces preserves inoculum composition and richness

(A) Experimental setup. Germ-free mice colonized with feces from a single human donor ("humanized") were fed an SD or an MD and treated with ciprofloxacin for 5 days. Fecal samples from two mice on each diet were collected on 4 days (0, 1, 5, and 14) before, during, at the end of, and after treatment and were inoculated into anaerobic batch culture and passaged with dilution every 48 h to derive SICs. Sixteen samples (2 diets, 2 mice, and 4 time points during ciprofloxacin treatment) were inoculated into 4 media (BHI, TYG, GAM, and YCFA) in triplicate.

(B) Diet alters the trajectory of microbiota reorganization during ciprofloxacin treatment *in vivo*. PCoA of community composition of the fecal inocula using unweighted Unifrac distance computed on all *in vivo* and *in vitro* samples at the ASV level. Lines (black and gray) correspond to two different mice.

(C) Medium and inoculum determine the final composition of passaged SICs. The 7th passage of all 192 SICs is shown in a PCoA of SIC composition using unweighted Unifrac distance computed on all *in vivo* and *in vitro* samples at the ASV level. Left: samples are colored by media, with shapes representing the diet in the mice from which the inocula were taken. Symbols are the centroid of three replicates, with lines connecting the replicates to the centroid. Right: SICs derived in BHI with colors and shapes representing the time point during ciprofloxacin treatment and diet, respectively, in the mice from which the inocula were taken. Symbols are the centroid of three replicates, with lines connecting the replicates to the centroid. Original fecal inocula are plotted in light colors.

(D) Most steady-state SICs are similar to the fecal samples from which they were derived, as shown by weighted Unifrac distance of the 7th passage of each SIC to the corresponding fecal inoculum. Colored circles, mean distance for each medium; individual SICs in gray. Error bars, standard deviations; n = 48. Dashed line, mean distance between fecal samples.

(E) SIC diversity correlates with inoculum diversity in BHI. Richness (number of ASVs in rarefied data) was compared for the 7th passage of each SIC and the corresponding fecal inoculum, and separated and colored/shaped as in (C). *R* and p are for Pearson coefficient; n = 48.

B

C

D

E

inoculum. Indeed, the richness of SICs grown in BHI, TYG, and GAM was highly correlated with that of the inoculum, with some SICs having >50 detectable ASVs (Figures 3E and S5F).

Since BHI-passaged SICs were more compositionally similar to their inocula than SICs derived in other media (Figures 3C and 3D), we focused on these SICs and queried the extent to which their richness was due to species that were detectable in the inoculum as opposed to emergent species that increased above the limit of detection due to passaging. While almost 40% of the ASVs detected in the inoculum were maintained, there were also 22.0 ± 3.0 ASVs detected in SICs that were undetectable in the inoculum, which could be due to contamination or to a jump in abundance during passaging from below to above the limit of detection. The lack of contamination in control wells in our plates, along with the observation that replicates exhibited many of the same emergent ASVs (63% of the 27 emergent ASVs were present in all three replicates), suggested that contamination was generally low. These observations are reminiscent of the emergence of *A. muciniphila* within mice switched from a SD to a MD, even though these bacteria were often undetectable before the dietary switch (Earle et al., 2015). Most emergence in our SICs was due to within-family replacement; the only emergent family was the sole Gammaproteobacteria in the SIC (an Enterobacteriaceae) that had no detectable members in the inoculum. The ASVs that emerged typically did so in all three replicates, further underscoring the deterministic nature of SIC dynamics even at low abundance. As a whole, emergent ASVs accounted for 44.6% ± 0.9% of the SIC, with 29.1% ± 2.5% due to the Enterobacteriaceae ASV, and their median $\log_{10}$(relative abundance) in the SICs was similar to that of the ASVs that were retained (−2.13 and −2.14, respectively; p = 0.35, Wilcoxon test). Emergent ASVs reached stable levels, defined as within 2 standard deviations of their mean $\log_{10}$(relative abundance) beyond the fourth passage, in 2.05 ± 1.22 passages. These data suggest that the emergence of an ASV does not predict its abundance in the SIC and that restructuring of SICs (both loss and emergence) primarily occurs in the first two passages.

The total number of ASVs present in at least one inoculum (fecal gamma diversity) was 158, of which 68 were present in at least one BHI SIC and 79 in any medium. The total number of ASVs present in at least one SIC was 117. Of these, two appeared in at least one technical replicate of all BHI SICs, an *Enterococcus* species and a member of the Lachnospiraceae family; four more Lachnospiraceae were included when we ignored the low-diversity SIC cultured from residual treatment inoculum. Intriguingly, these ASVs were present in the core microbiota of almost all mice at the point of minimum alpha diversity during antibiotic treatment (Ng et al., 2019), suggesting their general ability to persist through perturbations.

Species loss and emergence were ubiquitous across all SICs in all media. The fraction of ASVs detectable in the fecal sample that remained detectable in the 7th passage was negatively correlated with the diversity of the inoculum (for BHI, $R = -0.89$, p = 10^{-17}; Figure S6A), consistent with our observation that less-abundant members are more likely to disappear. Conversely, the fraction of emergent ASVs was positively correlated with the diversity of the inoculum ($R = 0.61$, p = 10^{-6}, Figure S6B). However, the fraction of families lost was weakly anticorrelated with inoculum diversity (Fig-

ure S6C), and the fraction of families that emerged was also weakly anticorrelated with inoculum diversity (Figure S6D), indicating general species replacement within families. Almost 90% of the ASVs that were lost or gained did so within the first four passages (Figures S6E and S6F). More than 66% of lost ASVs went undetectable from all the inocula in which they were present, indicating that most of the disappearance dynamics were deterministic. While *A. muciniphila* was present in all inocula, it was maintained in 16.7% of all SICs and in 31.3% of BHI SICs, albeit at decreased relative abundance compared to the inoculum.

Exposure to ciprofloxacin *in vivo* increases *Salmonella* invasion *in vitro*

The compositions of SICs derived during and after antibiotic treatment resembled the compositions of the inocula (Figures 3B and 3C). Thus, we next asked whether the SICs recapitulated an important feature observed *in vivo*: decreased resistance to colonization by the pathogen *Salmonella enterica* serovar Typhimurium (Barthel et al., 2003; Lawley et al., 2008). Specifically, we asked whether exposure to ciprofloxacin led to compositional changes that reduce colonization resistance in the absence of the drug *in vitro*. We grew SICs derived from SD mice inocula gathered before, during the peak of, during residual, and after treatment *in vivo* (Pre-SD, Peak-SD, Res-SD, and Post-SD, respectively) in BHI. We challenged these SICs with *S*. Typhimurium for 48 h in BHI, diluted them, spotted them onto LB-streptomycin agar plates, and incubated them in aerobic conditions to select for *S*. Typhimurium (Figure 4A). Pre-SD SICs had >10-fold less *S*. Typhimurium than communities derived from feces of ciprofloxacin-treated mice (Figures 4B and S7A). Single-cell quantification of fluorescently tagged *S*. Typhimurium revealed an even larger difference in colonization efficiency between the Pre-SD and Res-SD SICs (Figures 4C and S7B). Thus, changes in composition driven by antibiotic treatment *in vivo* lead to differences in SICs that mimic the resilience of the microbiota to *S*. Typhimurium invasion *in vivo*.

Ciprofloxacin alters SICs in a manner consistent with isolate sensitivities and *in vivo* dynamics

We isolated 15 strains from a Pre-MD SIC and measured their MICs (Table S1). The Lachnospiraceae exhibited the highest MICs (Figure 5A), consistent with the high levels of Lachnospiraceae and Ruminococcaceae in humanized mice at the peak of ciprofloxacin treatment (Figure S2B). Most sensitive families (minimum inhibitory concentration [MIC] < 32 μg/mL) decreased in abundance *in vivo* (Figure 5A); the lone exception was the Bacteroidaceae, which increased in three of four mice (Figure 5A), consistent with our previous observation that a highly resistant *Bacteroides vulgatus* strain (MIC > 512 μg/mL) can be selected *in vivo* (Ng et al., 2019). These results suggest that ciprofloxacin sensitivities are generally similar *in vitro* and *in vivo*.

We next queried the responses of a Pre-SD SIC to ciprofloxacin (Figure 5B). The maximum growth rate of the SIC decreased monotonically with drug concentration (Figure 5C) and the collective MIC for the SIC was >32 μg/mL (Figure 5C). To assess the effects of long-term exposure to ciprofloxacin on SIC composition, we passaged the Pre-SD SIC in BHI with ciprofloxacin twice more (Figures 5Bii and 5Biii). The maximum growth
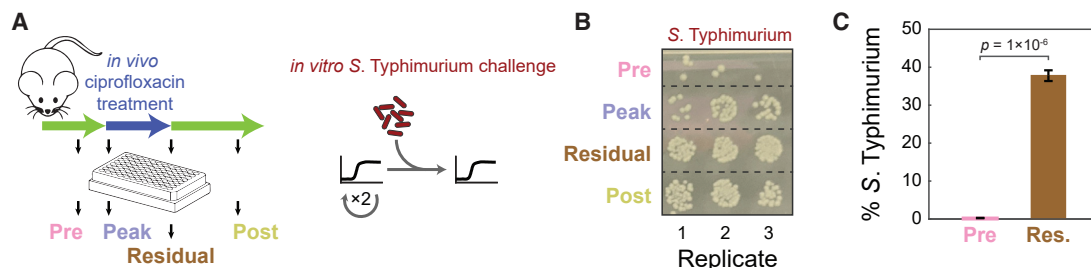
Figure 4. Pre-exposure of the gut microbiota to ciprofloxacin *in vivo* results in differential invasion of *S.* Typhimurium *in vitro*
(A) Experimental setup for *in vitro* challenge with *S.* Typhimurium. SICs passaged in BHI from pre-, peak, residual, and post-treatment humanized mouse fecal inocula were revived after freezing and passaged twice in BHI. SICs were mixed with *S.* Typhimurium, and *S.* Typhimurium levels were quantified after 48 h of growth.
(B) SICs derived from mice treated with ciprofloxacin are more susceptible to *S.* Typhimurium. Colonies of *S.* Typhimurium SL1344 after 48 h of growth with SICs diluted 1:10^4 and grown aerobically on LB + streptomycin.
(C) Single-cell quantification of mCherry-tagged *S.* Typhimurium 14028s after co-culture with SICs derived from pre- and residual treatment mice fecal inocula. The p-value is from a Student's two-sided t-test; n = 3.

rate of the SICs remained low, suggesting that community re-modeling took place during the first ciprofloxacin passage (Figure S7C). At 2 μg/mL, diversity decreased steadily (Figure 5D); at 32 μg/mL, diversity declined to lower levels than untreated SICs derived from the residual treatment inoculum (Figures 5D and S7C). For all doses, many families decreased to undetectable levels, including the abundant Enterobacteriaceae and Enterococcaceae (Figure 5E), while members of the Lachnospiraceae, Ruminococcaceae, and Bacteroidaceae persisted after three rounds in 2 and 8 μg/mL ciprofloxacin (Figure 5E). At 32 μg/mL, the Ruminococcaceae were undetectable by the second passage and the Bacteroidaceae decreased to very low levels (Figure 5E), likely explaining the large decrease in maximum optical density (OD) relative to 16 μg/mL (Figure 5C).

Antibiotic pressure selected for strains that emerged from below the detection limit due to the decrease of other, more sensitive species: at 2 μg/mL the Lachnospiraceae increased from 12 to 16 detectable ASVs while the Bacteroidaceae decreased from 12 to 4 detectable ASVs. This emergence was not due to contamination: at every concentration, changes were highly reproducible between replicates (>89% and >69% of ASVs that became undetectable or detectable, respectively, did so in both replicates). Moreover, the MICs of the 15 isolates were highly correlated with the fractional change in abundance upon 2 μg/mL ciprofloxacin treatment of the Pre-SD SIC (Figure 5F). Hence, the compositional changes observed in SICs can largely be predicted by individual sensitivities in isolation.

SICs derived from pre-exposed inocula show increased resilience to ciprofloxacin treatment

To determine whether pre-exposed SICs show increased resilience to ciprofloxacin treatment *in vitro*, we selected a low diversity SIC derived from an SD mouse inoculum during residual treatment *in vivo* (Res-SD, Figure S7D) and grew it in BHI with ciprofloxacin either continuously (Figures S7Di–S7Diii) or transiently (Figures S7Di, S7Div, and S7Dv). The Res-SD SIC was less sensitive than the Pre-SD SIC in terms of growth rate (Figures 5C and S7E), and the final OD was largely unaffected (Figure S7E). These data suggest that the Res-SD SIC derived

from the feces of antibiotic-treated mice is less susceptible to ciprofloxacin.

We next asked whether the robustness of Res-SD SIC growth behaviors during ciprofloxacin treatment could be explained by particular compositional differences with the Pre-SD SIC. The Res-SD SIC displayed distinct responses compared with the Pre-SD SIC, maintaining its diversity even at the highest ciprofloxacin concentrations (Figures 5D and S7F). At all concentrations, Bacteroidaceae and Lachnospiraceae dominated, even after three passages (Figure S7G), in contrast to the decrease of most Bacteroidaceae members in the Pre-SD SIC (Figure 5E). The most abundant lost family from Res-SD SIC was the Enterococcaceae (Figure S7G); the Ruminococcaceae and Verrucomicrobiaceae were lost at 32 and 2 μg/mL, respectively. These losses were counterbalanced by emergent ASVs within the resistant families. The composition was quantitatively similar at the ASV level between the two replicates at low concentrations (Figure S7H). At 32 μg/mL, the two replicates were more similar to each other than the Pre-SD SIC after treatment (Figure S7I), suggesting that pre-exposure to the drug in mice decreases the stochastic nature of species elimination upon subsequent exposure *in vitro*. The composition of the Res-SD SIC before treatment and after two recovery passages were highly similar at low doses (Figure S7J). These data imply that the members of the Res-SD SIC are more resistant to the drug, in line with their pre-selection *in vivo*.

SICs successfully predict *in vivo* compositional changes due to ciprofloxacin

Drug concentration is typically hard to determine along the gastrointestinal tract and potentially heterogeneous in space and time. Other variables are also difficult to measure and control, such as environmental reservoirs that play a role in bacterial migration and repopulation. The SICs we generated from antibiotic-treated mice provide the opportunity to study antibiotic perturbations in a precisely controlled and high-throughput manner and to assess similarity to *in vivo* behavior.

In vivo, the microbiota undergoes a complex recovery that likely involves differential susceptibilities, intrinsic recovery capacities, the emergence of resistant mutants, and metabolic
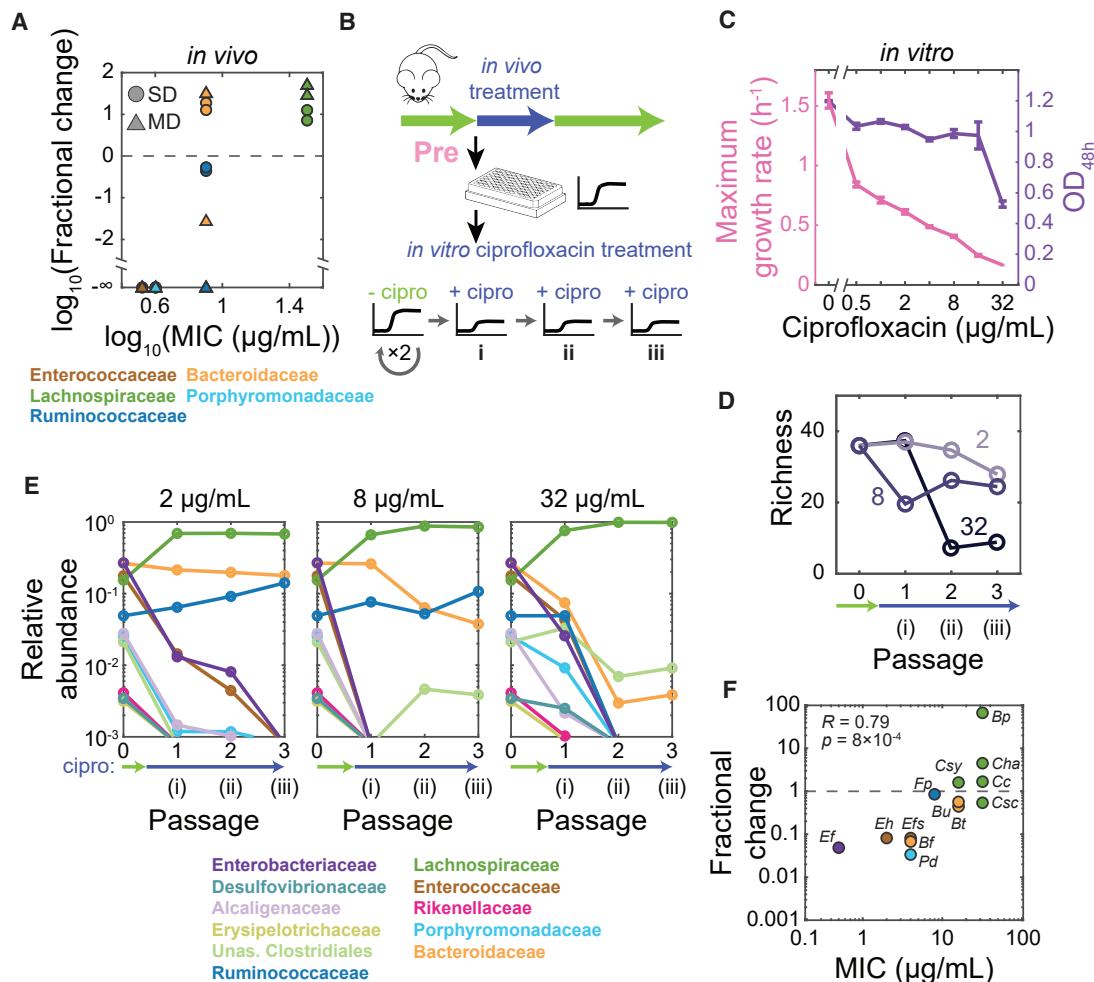
Figure 5. *In vitro* treatment of an SIC with ciprofloxacin results in changes in community composition consistent with strain sensitivity

(A) Changes in family-level abundances during ciprofloxacin treatment *in vivo* can be predicted by strain-level sensitivities *in vitro*. Fractional changes were computed as the ratio of residual and pre-treatment time point abundances *in vivo*. MIC is the mean value across strains in a given family, determined from growth in isolation in BHI (Table S1).

(B) Experimental setup. An SIC passaged in BHI from a pre-treatment humanized mouse fecal inoculum (Pre-SD) was passaged in ciprofloxacin three times (Bi–Biii).

(C) Pre-SD SIC yield and growth rate decreased with increasing concentrations of ciprofloxacin. OD was measured after 48 h of growth with ciprofloxacin. Lines, means of triplicate growth curves; error bars, standard deviations.

(D) Richness of the Pre-SD SIC decreased in a dose-dependent manner. Data are means of two technical replicates.

(E) Ciprofloxacin treatment *in vitro* selects for a few families. Family-level composition of the Pre-SD SIC across passages in ciprofloxacin. The limit of detection was $\sim 10^{-3}$. Data are means of two technical replicates.

(F) Growth of ASVs in the Pre-SD SIC under ciprofloxacin treatment can be predicted by their sensitivity in isolation. Fractional-abundance changes of ASVs corresponding to the 15 isolates in (A) were computed after one passage in 2 μg/mL ciprofloxacin.

interactions (Ng et al., 2019). To investigate the response of SICs in conditions mimicking recovery, after one round in ciprofloxacin, we diluted the Pre-SD SIC into BHI without ciprofloxacin (Figures 6Ai, 6Aiv, and 6Av). Maximum growth rate increased after one round of treatment at all doses (Figure S7K); at low doses, growth rate rebounded to values similar to those before treatment, while at >8 μg/mL it only partially recovered (Figure S7K), likely due to extinction of the Enterococcaceae (Figure S7L; Table S1). Diversity increased slightly after drug removal (Figure 6B), suggesting the recovery of certain species from below the limit of detection. Thus, diversity recovery *in vitro* (Figure 6B)

can be partially explained by re-emergence of ASVs that became undetectable but not extinct during treatment.

The small increase in SIC diversity after ciprofloxacin removal (Figure 6B) involved recovery of Erysipelotrichaceae members from below the limit of detection (Figure 6C), consistent with its recovery *in vivo* (Figures 6D and 6E). A second treatment after one passage without the drug again made the Erysipelotrichaceae undetectable (Figure S7M), indicating that sensitivity to ciprofloxacin was unchanged. The Ruminococcaceae exhibited recovery (Figure 6C), unsurprisingly since they also survived continued treatment at intermediate concentrations (Figure 5E).
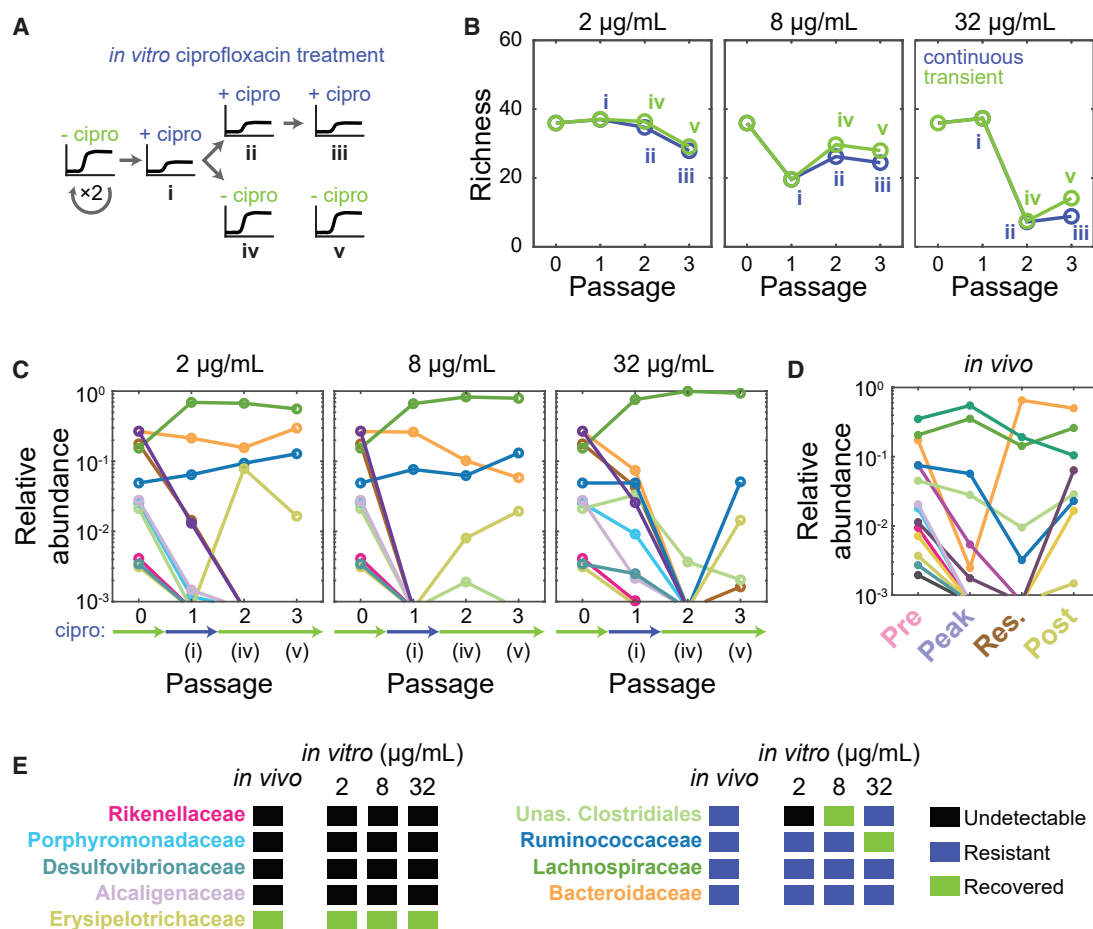
Figure 6. *In vitro* treatment of an SIC with ciprofloxacin results in similar responses as *in vivo*
(A) Experimental setup mimicking transient treatment *in vivo*. An SIC passaged in BHI from a pre-treatment humanized mouse fecal inoculum (Pre-SD) was passaged in ciprofloxacin three times (Ai–Aiii), or in ciprofloxacin once and then twice without the drug (Ai, Aiv, and Av).
(B) Richness of the Pre-SD SIC recovered only partially after removal of ciprofloxacin (green) versus continuous exposure (blue). Data are means of two technical replicates.
(C) Some families (e.g., Erysipelotrichaceae and Ruminococcaceae) recover after transient ciprofloxacin treatment. Data are the mean $\log_{10}$(relative abundance) at the family level of two replicates during one round of ciprofloxacin treatment and two rounds of recovery.
(D) Ciprofloxacin-induced changes to family-level abundances in SD mice *in vivo* resemble changes *in vitro* in (C). Data are the mean $\log_{10}$(relative abundance) at the family level of two mice.
(E) Most families display similar qualitative abundance changes *in vivo* and *in vitro*.

The other families did not recover from undetectable levels after removing the drug *in vitro* or *in vivo* (Figures 6D and 6E). Taken together, these results suggest that *in vitro* perturbations can be used as a proxy for many aspects of *in vivo* dynamics.

***Bacteroides* recovery *in vitro* is due to a combination of resistance and resilience**
The unexpected recovery of the Bacteroidaceae *in vivo* motivated us to probe the dynamics of these ASVs. *In vivo*, although most *Bacteroides* ASVs were undetectable at the peak and residual time points, most reappeared post-treatment (Figure 7A). Only *B. vulgatus* increased in relative abundance to become dominant during residual treatment (Figure 7B); this strain was likely highly resistant to ciprofloxacin based on our assessment of *Bacteroides* isolates from the residual fecal sample (Ng et al., 2019). Consistent with this observation, *B. vulgatus* was

the only Bacteroidaceae ASV present *in vitro* after 3 passages with 32 µg/mL ciprofloxacin, reaching a stable abundance in the Pre-SD (Figure 7B) and Res-SD SICs (Figure S7N). *B. caccae* and *B. uniformis* were present after 3 passages of the Pre-SD SIC at 8 µg/mL, and *B. thetaiotaomicron* was present after 3 passages at 2 µg/mL (Figure 7B); all three species recovered *in vivo* post-treatment (Figure 7A), which our data suggest is due to their intrinsic resistance. Other *Bacteroides* species, such as *B. fragilis*, became undetectable after one passage at 2 µg/mL in both SICs (Figures 7B and S7N). These trends are consistent with the higher MICs of *B. uniformis* and *B. thetaiotaomicron* compared with *B. fragilis* (Table S1). Thus, sensitivities of isolates are predictive of *Bacteroides* resistance during continuous ciprofloxacin treatment.

Similar to *B. fragilis*, *B. intestinalis* was undetectable by the second passage, even at 2 µg/mL (Figure 7B). Nonetheless,
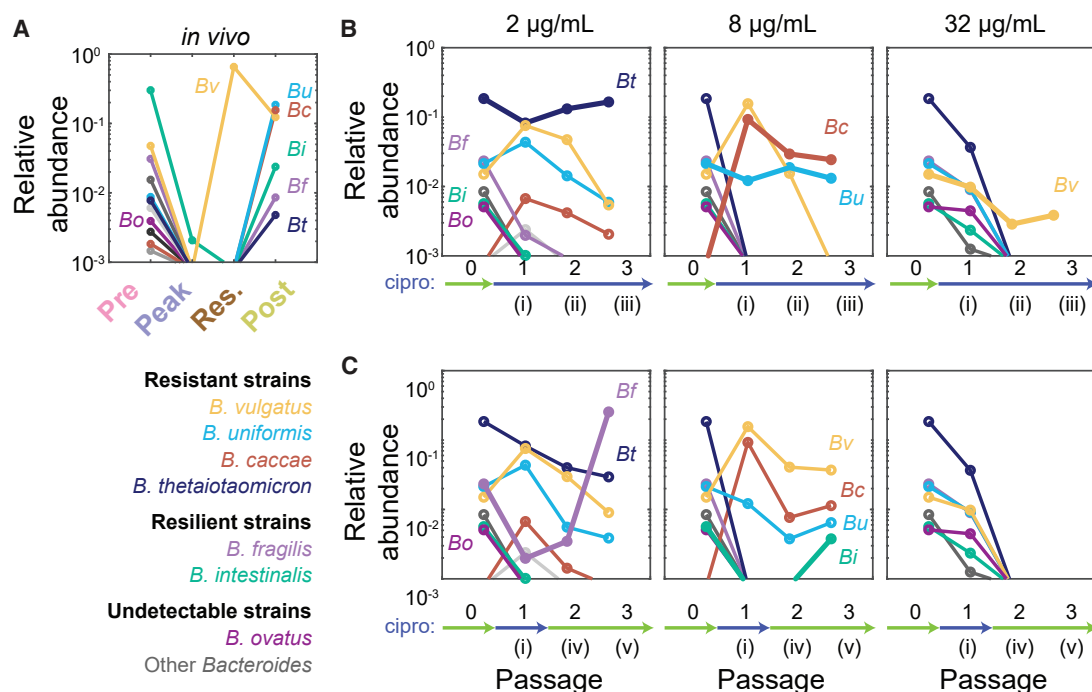
Figure 7. *In vitro* treatment of an SIC reveals resistance and resilience in the *Bacteroides* genus

(A) *Bacteroides* dynamics *in vivo* consist of *B. vulgatus* dominance during treatment and the recovery of several species after treatment. Data are the mean log$_{10}$(relative abundance) at the ASV level across two SD mice: *Bacteroides ovatus* (*Bo*), *B. vulgatus* (*bv*), *B. uniformis* (*Bu*), *B. caccae* (*Bc*), *B. intestinalis* (*Bi*), *B. fragilis* (*Bf*), and *B. thetaiotaomicron* (*Bt*). Other *Bacteroides* are shown in shades of gray.

(B and C) *Bacteroides* survival and recovery *in vivo* can be explained by resistance and resilience characteristics of the Pre-SD SIC *in vitro* during continuous treatment (B) or one round of treatment followed by two rounds of recovery (C), respectively. Data are the mean log$_{10}$(relative abundance) of two replicates during one round of ciprofloxacin treatment and two rounds of recovery at the ASV level. Thick lines highlight *Bacteroides* ASVs that show resistance (B) or resilience (C) at the highest concentration that they display the behavior.

both species recovered *in vivo* in SD mice (Figure 7A). Remarkably, these species also re-emerged *in vitro* upon further passage without the drug in the Pre-SD SIC (Figure 7C), as did *B. fragilis* in the Res-SD SIC (Figure S7O). In fact, *B. fragilis* became dominant after recovery from treatment with 2 μg/mL in the Pre-SD SIC (Figure 7C), similar to the replacement of resistant *B. vulgatus in vivo* by other *Bacteroides* (Ng et al., 2019), and consistent with dominance of *B. fragilis* in the Res-SD SIC (Figure S7N). *B. intestinalis* was detected in the Pre-SD SIC only after recovery from treatment with 8 μg/mL (Figure 7C), suggesting that different ciprofloxacin concentrations can alter the competitive landscape of *Bacteroides* species. We refer to the ability of strains to recover from undetectable levels during treatment as "resilience." Interestingly, *B. vulgatus* was only detected when the SIC was continuously exposed (Figure 7B) and not after ciprofloxacin was removed (Figure 7C), suggesting that recovery of other families can drive resistant members to undetectable levels. Species that did not recover *in vivo*, such as *B. ovatus*, did not recover *in vitro* (Figures 7A and 7C). In sum, fecal-derived SICs can distinguish between resistance and resilience.

DISCUSSION

In vitro co-culturing has proven instrumental in enhancing our understanding of microbial ecology, affording the ability to design consortia through combinatorial culturing and providing the po-

tential to capitalize on bacterial genetics for functional modifications of individual members. Here, we have shown that *in vitro* passaging of fecal samples is a complementary and powerful tool for generating stable, reproducible, complex SICs. Our approach yields complex SICs with >50 species, and it is likely possible to further increase SIC diversity in media supplemented with specific nutrients that promote the growth of fastidious organisms (Tramontano et al., 2018). While YCFA supports the growth of a wide range of gut commensals in isolation, in SICs the Enterococcaceae take over (Figures S5A and S5C), indicating that media that support isolate growth do not necessarily support diverse SICs. Improved understanding of the contributions of interspecies interactions and nutrient availability to community assembly will be instrumental to engineering future gut models, and SICs represent a major step toward this goal.

Our study shows that SICs can shed light on behaviors observed *in vivo*. SICs derived from mice during and after antibiotic treatment were more susceptible to invasion by *S.* Typhimurium than SICs derived before treatment (Figure 4). While previous studies reported that ciprofloxacin treatment can increase the colonization susceptibility of chemostat-grown microbial communities (Carman et al., 2004), our experiments were conducted in the absence of ciprofloxacin at the time of challenge. Thus, the compositional changes elicited by antibiotics *in vivo* are maintained *in vitro*, leading to different functional outcomes. Our quantitative comparison between the ciprofloxacin

response of the gut microbiota *in vivo* and *in vitro* revealed remarkable similarities in taxon-specific changes in diversity (Figure 6E), despite differences in spatial structure, duration of treatment, and population sizes between SICs and the gut. Thus, SICs have the potential to shed light on many aspects of the dynamics that are confounded by multiple factors *in vivo*. The observed correlation between abundance changes upon continuous ciprofloxacin treatment and strain sensitivities (Figure 5F) suggests that interspecies interactions are not strong modifiers of ciprofloxacin sensitivity in these communities. Nevertheless, the predicted emergence of resistant strains led to a subsequent out-competition by close relatives upon removal of the drug, highlighting the role of ecological interactions on community structure. Further studies using SICs can elucidate the role of ecology on antibiotic sensitivity and community structure, especially in the case of antibiotics where indirect resistance can benefit multiple species (Brook, 2009; Sorg et al., 2016). The lack of substantial recovery in richness *in vitro* after treatment (Figure 6B) suggests that the ~4-fold increase *in vivo* post-treatment (Figure S2C) could come from environmental re-seeding, supporting the physiological relevance of reservoirs suggested *in vivo* by comparisons of singly housed and co-housed mice (Ng et al., 2019). Nonetheless, the recovery *in vitro* of some species such as *B. intestinalis* from undetectable levels did not require reseeding (Figure 7C), indicating built-in resilience; such findings point to the ability of SICs to elucidate aspects of community ecology that can be uncoupled from host dependence. Taken together, this study indicates that dissecting how a gut community is remodeled by a perturbation *in vitro* can serve as a pre-screening tool before expensive animal experiments. Many other fascinating questions should be tackled in the future using our *in vitro* approach, which can easily be scaled to thousands of communities.

SIC colonization of germ-free mice largely resulted in the same composition and shifted the host proteome of germ-free mice toward that of humanized mice (Figures 2B–2E). Moreover, the observation that fast-growing species expand in SICs (Figures 1B and 1C) but recede in SIC-colonized mice (Figure 2B) reveals the few bacterial taxa whose growth is controlled by the host, highlighting further importance of *in vitro* models. These results suggest the potential of personalized SICs to study community function and its relationship with perturbations and the host, as well as to develop scalable and safe therapeutic alternatives to fecal microbiota transplants (Khoruts and Weingarden, 2014). A combination of top-down and bottom-up stool-derived communities should serve as powerful, complementary resources for the microbiota field. More generally, SICs may provide a bridge between mechanistic studies of microbial ecology and human-relevant *in vivo* systems.

STAR★METHODS

Detailed methods are provided in the online version of this paper and include the following:

- KEY RESOURCES TABLE
- RESOURCE AVAILABILITY
  - ○ Lead contact
  - ○ Materials availability

  - ○ Data and code availability
- EXPERIMENTAL MODEL AND SUBJECT DETAILS
  - ○ Mouse strains
  - ○ Human subjects
  - ○ Bacterial strains
- METHOD DETAILS
  - ○ Mouse humanization and fecal sampling
  - ○ SIC passaging, storage, and revival
  - ○ SIC colonization
  - ○ Strains and growth media
  - ○ 16S rRNA gene sequencing
  - ○ Isolation of strains
  - ○ Antibiotic sensitivity estimation
  - ○ *In vitro Salmonella* Typhimurium challenge
  - ○ *In vitro* antibiotic treatment
  - ○ Isolation of stool proteins and peptides
  - ○ Mass spectrometry
  - ○ Peptide/protein database searching
- QUANTIFICATION AND STATISTICAL ANALYSIS
  - ○ 16S data analysis
  - ○ Growth analyses
  - ○ Proteome analysis
  - ○ Bacterial invasion
  - ○ Statistical analyses

SUPPLEMENTAL INFORMATION

Supplemental information can be found online at https://doi.org/10.1016/j.chom.2021.12.008.

AUTHOR CONTRIBUTIONS

A.A.-D., K.M.N., J.L.S., and K.C.H. designed the research; A.A.-D., K.M.N., T.T., I.R.-R., D.D., S.D., C.G.G., T.C., K.S.V., T.H.N., F.B.Y., and S.K.N. performed the research; A.A.-D., K.M.N., D.D., and C.G.G. analyzed the data; A.A.-D., J.L.S., and K.C.H. wrote the paper, and all authors reviewed it before submission.

DECLARATION OF INTERESTS

The authors declare no competing interests.

SUPPORTING CITATIONS

The following references appear in the supplemental information: Duncan et al., 2002.

REFERENCES

Adamowicz, E.M., Flynn, J., Hunter, R.C., and Harcombe, W.R. (2018). Cross-feeding modulates antibiotic tolerance in bacterial communities. ISME J *12*, 2723–2735.

Aranda-Díaz, A., Obadia, B., Thomsen, T., Hallberg, Z.F., Güvener, Z.T., Ludington, W.B., and Huang, K.C. (2020). Bacterial interspecies interactions modulate pH-mediated antibiotic tolerance. Elife *9*, e51493.

Auchtung, J.M., Robinson, C.D., Farrell, K., and Britton, R.A. (2016). MiniBioReactor arrays (MBRAs) as a tool for studying *C. difficile* physiology in the presence of a complex community. Methods Mol. Biol. *1476*, 235–258.

Barroso-Batista, J., Pedro, M.F., Sales-Dias, J., Pinto, C.J.G., Thompson, J.A., Pereira, H., Demengeot, J., Gordo, I., and Xavier, K.B. (2020). Specific eco-evolutionary contexts in the mouse gut reveal *Escherichia coli* metabolic versatility. Curr. Biol. *30*, 1049–1062.e7.

Barthel, M., Hapfelmeier, S., Quintanilla-Martínez, L., Kremer, M., Rohde, M., Hogardt, M., Pfeffer, K., Rüssmann, H., and Hardt, W.-D. (2003). Pretreatment of mice with streptomycin provides a *Salmonella enterica* serovar Typhimurium colitis model that allows analysis of both pathogen and host. Infect. Immun. *71*, 2839–2858.

Brook, I. (2009). The role of beta-lactamase-producing-bacteria in mixed infections. BMC Infect. Dis. *9*, 202.

Browne, H.P., Forster, S.C., Anonye, B.O., Kumar, N., Neville, B.A., Stares, M.D., Goulding, D., and Lawley, T.D. (2016). Culturing of "unculturable" human microbiota reveals novel taxa and extensive sporulation. Nature *533*, 543–546.

Callahan, B.J., McMurdie, P.J., Rosen, M.J., Han, A.W., Johnson, A.J., and Holmes, S.P. (2016). DADA2: high-resolution sample inference from Illumina amplicon data. Nat. Methods *13*, 581–583.

Caporaso, J.G., Kuczynski, J., Stombaugh, J., Bittinger, K., Bushman, F.D., Costello, E.K., Fierer, N., Peña, A.G., Goodrich, J.K., Gordon, J.I., et al. (2010). QIIME allows analysis of high-throughput community sequencing data. Nat. Methods *7*, 335–336.

Carman, R.J., Simon, M.A., Fernández, H., Miller, M.A., and Bartholomew, M.J. (2004). Ciprofloxacin at low levels disrupts colonization resistance of human fecal microflora growing in chemostats. Regul. Toxicol. Pharmacol. *40*, 319–326.

Cho, I., Yamanishi, S., Cox, L., Methé, B.A., Zavadil, J., Li, K., Gao, Z., Mahana, D., Raju, K., Teitler, I., et al. (2012). Antibiotics in early life alter the murine colonic microbiome and adiposity. Nature *488*, 621–626.

Cox, L.M., Yamanishi, S., Sohn, J., Alekseyenko, A.V., Leung, J.M., Cho, I., Kim, S.G., Li, H., Gao, Z., Mahana, D., et al. (2014). Altering the intestinal microbiota during a critical developmental window has lasting metabolic consequences. Cell *158*, 705–721.

de Vos, M.G.J., Zagorski, M., McNally, A., and Bollenbach, T. (2017). Interaction networks, ecological stability, and collective antibiotic tolerance in polymicrobial infections. Proc. Natl. Acad. Sci. USA *114*, 10666–10671.

Dethlefsen, L., and Relman, D.A. (2011). Incomplete recovery and individualized responses of the human distal gut microbiota to repeated antibiotic perturbation. Proc. Natl. Acad. Sci. USA *108* (*Suppl. 1*), 4554–4561.

Duncan, S.H., Hold, G.L., Harmsen, H.J.M., Stewart, C.S., and Flint, H.J. (2002). Growth requirements and fermentation products of *Fusobacterium prausnitzii*, and a proposal to reclassify it as *Faecalibacterium prausnitzii* gen. nov., comb. nov. Int. J. Syst. Evol. Microbiol. *52*, 2141–2146.

Earle, K.A., Billings, G., Sigal, M., Lichtman, J.S., Hansson, G.C., Elias, J.E., Amieva, M.R., Huang, K.C., and Sonnenburg, J.L. (2015). Quantitative imaging of gut microbiota spatial organization. Cell Host Microbe *18*, 478–488.

Faith, J.J., McNulty, N.P., Rey, F.E., and Gordon, J.I. (2011). Predicting a human gut microbiota's response to diet in gnotobiotic mice. Science *333*, 101–104.

Fröhlich, E.E., Farzi, A., Mayerhofer, R., Reichmann, F., Jačan, A., Wagner, B., Zinser, E., Bordag, N., Magnes, C., Fröhlich, E., et al. (2016). Cognitive impairment by antibiotic-induced gut dysbiosis: analysis of gut microbiota-brain communication. Brain Behav. Immun. *56*, 140–155.

Goldford, J.E., Lu, N., Bajić, D., Estrela, S., Tikhonov, M., Sanchez-Gorostiaga, A., Segrè, D., Mehta, P., and Sanchez, A. (2018). Emergent simplicity in microbial community assembly. Science *361*, 469–474.

Gonzalez, C.G., Wastyk, H.C., Topf, M., Gardner, C.D., Sonnenburg, J.L., and Elias, J.E. (2020). High-throughput stool metaproteomics: method and application to human specimens. mSystems *5*, e00200–e00220.

Gutiérrez, N., and Garrido, D. (2019). Species deletions from microbiome consortia reveal key metabolic interactions between gut microbes. mSystems *4*, e00185–e00119.

Hooper, L.V., Littman, D.R., and Macpherson, A.J. (2012). Interactions between the microbiota and the immune system. Science *336*, 1268–1273.

Hwang, I., Park, Y.J., Kim, Y.R., Kim, Y.N., Ka, S., Lee, H.Y., Seong, J.K., Seok, Y.J., and Kim, J.B. (2015). Alteration of gut microbiota by vancomycin and bacitracin improves insulin resistance via glucagon-like peptide 1 in diet-induced obesity. FASEB J *29*, 2397–2411.

Ivanov, I.I., Frutos, R.D.L., Manel, N., Yoshinaga, K., Rifkin, D.B., Sartor, R.B., Finlay, B.B., and Littman, D.R. (2008). Specific microbiota direct the differentiation of IL-17-producing T-helper cells in the mucosa of the small intestine. Cell Host Microbe *4*, 337–349.

Johansson, M.E., Jakobsson, H.E., Holmén-Larsson, J., Schütte, A., Ermund, A., Rodríguez-Piñeiro, A.M., Arike, L., Wising, C., Svensson, F., Bäckhed, F., and Hansson, G.C. (2015). Normalization of host intestinal mucus layers requires long-term microbial colonization. Cell Host Microbe *18*, 582–592.

Kashyap, P.C., Marcobal, A., Ursell, L.K., Larauche, M., Duboc, H., Earle, K.A., Sonnenburg, E.D., Ferreyra, J.A., Higginbottom, S.K., Million, M., et al. (2013). Complex interactions among diet, gastrointestinal transit, and gut microbiota in humanized mice. Gastroenterology *144*, 967–977.

Kehe, J., Kulesa, A., Ortiz, A., Ackerman, C.M., Thakku, S.G., Sellers, D., Kuehn, S., Gore, J., Friedman, J., and Blainey, P.C. (2019). Massively parallel screening of synthetic microbial communities. Proc. Natl. Acad. Sci. USA *116*, 12804–12809.

Khoruts, A., and Weingarden, A.R. (2014). Emergence of fecal microbiota transplantation as an approach to repair disrupted microbial gut ecology. Immunol. Lett. *162*, 77–81.

Lawley, T.D., Bouley, D.M., Hoy, Y.E., Gerke, C., Relman, D.A., and Monack, D.M. (2008). Host transmission of *Salmonella enterica* serovar Typhimurium is controlled by virulence factors and indigenous intestinal microbiota. Infect. Immun. *76*, 403–416.

Lozupone, C., and Knight, R. (2005). UniFrac: a new phylogenetic method for comparing microbial communities. Appl. Environ. Microbiol. *71*, 8228–8235.

Lozupone, C.A., Hamady, M., Kelley, S.T., and Knight, R. (2007). Quantitative and qualitative beta diversity measures lead to different insights into factors that structure microbial communities. Appl. Environ. Microbiol. *73*, 1576–1585.

Macfarlane, G.T., Macfarlane, S., and Gibson, G.R. (1998). Validation of a three-stage compound continuous culture system for investigating the effect of retention time on the ecology and metabolism of bacteria in the human colon. Microb. Ecol. *35*, 180–187.

Mark Welch, J.L., Hasegawa, Y., McNulty, N.P., Gordon, J.I., and Borisy, G.G. (2017). Spatial organization of a model 15-member human gut microbiota established in gnotobiotic mice. Proc. Natl. Acad. Sci. USA *114*, E9105–E9114.

Mayer, E.A., Knight, R., Mazmanian, S.K., Cryan, J.F., and Tillisch, K. (2014). Gut microbes and the brain: paradigm shift in neuroscience. J. Neurosci. *34*, 15490–15496.

Minekus, M., Smeets-Peeters, M., Bernalier, A., Marol-Bonnin, S., Havenaar, R., Marteau, P., Alric, M., Fonty, G., and Huis In't Veld, J.H. (1999). A computer-controlled system to simulate conditions of the large intestine with peristaltic mixing, water absorption and absorption of fermentation products. Appl. Microbiol. Biotechnol. *53*, 108–114.

Ng, K.M., Aranda-Díaz, A., Tropini, C., Frankel, M.R., Van Treuren, W.W., O'Loughlin, C.T., Merrill, B.D., Yu, F.B., Pruss, K.M., Oliveira, R.A., et al. (2019). Recovery of the gut microbiota after antibiotics depends on host diet, community context, and environmental reservoirs. Cell Host Microbe *26*, 650–665.e4.

Ng, K.M., Ferreyra, J.A., Higginbottom, S.K., Lynch, J.B., Kashyap, P.C., Gopinath, S., Naidu, N., Choudhury, B., Weimer, B.C., Monack, D.M., and Sonnenburg, J.L. (2013). Microbiota-liberated host sugars facilitate post-antibiotic expansion of enteric pathogens. Nature *502*, 96–99.

Nicoloff, H., and Andersson, D.I. (2016). Indirect resistance to several classes of antibiotics in cocultures with resistant bacteria expressing antibiotic-modifying or -degrading enzymes. J. Antimicrob. Chemother. *71*, 100–110.

Rettedal, E.A., Gumpert, H., and Sommer, M.O. (2014). Cultivation-based multiplex phenotyping of human gut microbiota allows targeted recovery of previously uncultured bacteria. Nat. Commun. *5*, 4714.

Reyes, A., Wu, M., McNulty, N.P., Rohwer, F.L., and Gordon, J.I. (2013). Gnotobiotic mouse model of phage-bacterial host dynamics in the human gut. Proc. Natl. Acad. Sci. USA *110*, 20236–20241.

Rezzonico, E., Mestdagh, R., Delley, M., Combremont, S., Dumas, M.E., Holmes, E., Nicholson, J., and Bibiloni, R. (2011). Bacterial adaptation to the gut environment favors successful colonization: microbial and metabonomic characterization of a simplified microbiota mouse model. Gut Microbes *2*, 307–318.

Schubert, A.M., Sinani, H., and Schloss, P.D. (2015). Antibiotic-induced alterations of the murine gut microbiota and subsequent effects on colonization resistance against *Clostridium difficile*. mBio *6*, e00974.

Shi, H., Colavin, A., Lee, T.K., and Huang, K.C. (2017). Strain Library Imaging Protocol for high-throughput, automated single-cell microscopy of large bacterial collections arrayed on multiwell plates. Nat. Protoc. *12*, 429–438.

Sonnenburg, E.D., Smits, S.A., Tikhonov, M., Higginbottom, S.K., Wingreen, N.S., and Sonnenburg, J.L. (2016). Diet-induced extinctions in the gut microbiota compound over generations. Nature *529*, 212–215.

Sonnenburg, J.L., and Bäckhed, F. (2016). Diet-microbiota interactions as moderators of human metabolism. Nature *535*, 56–64.

Sorg, R.A., Lin, L., van Doorn, G.S., Sorg, M., Olson, J., Nizet, V., and Veening, J.W. (2016). Collective resistance in microbial communities by intracellular antibiotic deactivation. PLoS Biol *14*, e2000631.

Stecher, B., Robbiani, R., Walker, A.W., Westendorf, A.M., Barthel, M., Kremer, M., Chaffron, S., Macpherson, A.J., Buer, J., Parkhill, J., et al. (2007). *Salmonella enterica* serovar Typhimurium exploits inflammation to compete with the intestinal microbiota. PLoS Biol *5*, 2177–2189.

Tramontano, M., Andrejev, S., Pruteanu, M., Klünemann, M., Kuhn, M., Galardini, M., Jouhten, P., Zelezniak, A., Zeller, G., Bork, P., et al. (2018). Nutritional preferences of human gut bacteria reveal their metabolic idiosyncrasies. Nat. Microbiol. *3*, 514–522.

Tropini, C., Moss, E.L., Merrill, B.D., Ng, K.M., Higginbottom, S.K., Casavant, E.P., Gonzalez, C.G., Fremin, B., Bouley, D.M., Elias, J.E., et al. (2018). Transient osmotic perturbation causes long-term alteration to the gut microbiota. Cell *173*, 1742–1754.e17.

Venturelli, O.S., Carr, A.C., Fisher, G., Hsu, R.H., Lau, R., Bowen, B.P., Hromada, S., Northen, T., and Arkin, A.P. (2018). Deciphering microbial interactions in synthetic human gut microbiome communities. Mol. Syst. Biol. *14*, e8157.

Whitaker, W.R., Shepherd, E.S., and Sonnenburg, J.L. (2017). Tunable expression tools enable single-cell strain distinction in the gut microbiome. Cell *169*, 538–546.e12.

Zimmermann, M., Zimmermann-Kogadeeva, M., Wegmann, R., and Goodman, A.L. (2019). Separating host and microbiome contributions to drug pharmacokinetics and toxicity. Science *363*, eaat9931.

STAR★METHODS

KEY RESOURCES TABLE

REAGENT or RESOURCE	SOURCE	IDENTIFIER
Bacterial and virus strains		
Salmonella Typhimurium SL1344	Denise Monack lab, Stanford	SL1344
S. Typhimurium 14028s strain expressing cytoplasmic mCherry	Denise Monack lab, Stanford	N/A
Enterococcus hirae	This study	N/A
Escherichia fergusonii	This study	N/A
[Clostridium] symbiosum	This study	N/A
Bacteroides thetaiotaomicron	This study	N/A
[Clostridium] clostridioforme	This study	N/A
Blautia producta	This study	N/A
[Clostridium] scindens	This study	N/A
Enterococcus faecium	This study	N/A
[Clostridium] hylemonae	This study	N/A
Enterococcus faecalis	This study	N/A
[Clostridium] hathewayi	This study	N/A
Bacteroides fragilis	This study	N/A
Flavonifractor plautii	This study	N/A
Bacteroides uniformis	This study	N/A
Parabacteroides distasonis	This study	N/A
Chemicals		
Standard MAC-rich diet	Purina	LabDiet 5010
Defined low-MAC diet	Harlan	TD.86489
Ciprofloxacin	Sigma-Aldrich	17850
BHI medium	BD	2237500
Critical commercial assays		
DNeasy PowerSoil HTP 96 kit	Qiagen	12955-4
DNeasy UltraClean 96 Microbial kit	Qiagen	10196-4
Experimental models: organisms/strains		
Swiss Webster mice – germ-free	Taconic	SW GF
Critical Software		
DADA2 v. 1.14	Callahan et al., 2016	https://benjjneb.github.io/dada2/index.html
Qiime v.1.9.1	Caporaso et al., 2010	http://qiime.org/
Proteome Discoverer 2.2	Thermo Fisher	OPTON-30945
Oligonucleotides		
16S Sanger sequencing, forward	AGAGTTTGATCCTGGCTCAG	
16S Sanger sequencing, reverse	GACGGGCGGTGWGTRCA	
16S Illumina amplification, forward	AATGATACGGCGACCACCGAGATCTACACGCTNNNNNNNNNNNNTATGGTAATTGTGTGYCAGCMGCCGCGGTAA (N: 12 nucleotide barcode)	515f
16S Illumina amplification, reverse	CAAGCAGAAGACGGCATACGAGATAGTCAGCCAGCCGGACTACNVGGGTWTCTAAT	806rB
Read 1 sequencing primer	TATGGTAATTGTGTGYCAGCMGCCGCGGTAA	515fBC Read1

(Continued on next page)

Continued

REAGENT or RESOURCE	SOURCE	IDENTIFIER
Index sequencing primer	AATGATACGGCGACCACCGAGA TCTACACGCT	515fBC Index
Read 2 sequencing primer	AGTCAGCCAGCCGGACTACNVG GGTWTCTAAT	806rB Read2
Code		
Custom code used in this publication		DOI:10.5281/zenodo.570655410.5281/ zenodo.5706554

RESOURCE AVAILABILITY

Lead contact
Further information and requests for resources and reagents should be directed to and will be fulfilled by the lead contact, Kerwyn Casey Huang (kchuang@stanford.edu).

Materials availability
Bacterial communities described in this study can be requested from the lead contact. This study did not generate any other new unique reagents.

Data and code availability
All data reported in this paper will be shared by the lead contact upon request. Custom code used in this paper is available at doi:10.5281/zenodo.570655410.5281/zenodo.5706554. Any additional information required to reanalyze the data reported in this paper is available from the lead contact upon request.

EXPERIMENTAL MODEL AND SUBJECT DETAILS

Mouse strains
All mouse experiments were conducted in accordance with the Administrative Panel on Laboratory Animal Care, Stanford University's IACUC. Germ-free, Swiss-Webster mice were bred from an in-house colony and maintained in sterile incubators with food and water *ad libitum*. Females 6-12 weeks of age were cohoused (3-5 per cage). At the end of the experiments, mice were euthanized with CO_2, and death was confirmed via cervical dislocation.

Human subjects
Fecal samples were obtained from an anonymous donor (∼40 years old healthy white male).

Bacterial strains
Strains isolated from SICs and characterized in this study are listed in Table S1.

METHOD DETAILS

Mouse humanization and fecal sampling
Twenty germ-free mice (5 per cage) were gavaged with a human fecal sample obtained from a healthy male donor as previously described (Kashyap et al., 2013). The microbiota was allowed to equilibrate for 6-8 weeks before perturbation experiments commenced to allow for mucus normalization (Johansson et al., 2015). For experiments involving a dietary switch, mice were first fed a standard diet (Purina LabDiet 5010) rich in MACs, and then a defined low-MAC diet (Harlan TD.86489) in which the sole carbohydrates are sucrose (31% w/w), cornstarch (31% w/w), and cellulose (5% w/w) for two weeks to allow the microbiota to re-equilibrate. We then gavaged all mice (2 cages SD, 2 cages MD; *n*=20 total) for 5 days twice daily with 3 mg ciprofloxacin (Sigma Aldrich) dissolved in 200 μL of water. Since we previously showed that the responses of cage-mates to antibiotics are highly reproducible and stereotypical (Ng et al., 2019), we collected fecal samples from two randomly selected mice in different cages from each dietary condition on day 0 (pre-treatment) and on day 1 (peak of treatment, when the culturable load reached a maximum decrease of 10- to 100-fold (Ng et al., 2019)), day 5 (residual treatment, when ciprofloxacin was not being administered but was still detected in feces (Ng et al., 2019)), and day 14 (post-treatment). Fecal pellets were transported on ice and moved into an anaerobic chamber within 30 min.

SIC passaging, storage, and revival
Approximately 100 mg of stool samples from humanized mice or human donors were resuspended into 200 μL of phosphate-buffered saline (PBS) in 1.5-mL microcentrifuge tubes. Samples were incubated in PBS for 10-15 min at room temperature to encourage

large pieces of fecal matter to disintegrate. Samples were vortexed for 5 min and allowed to sit for 1 min to let food particles settle. One microliter of this resuspension was inoculated into 200 μL of medium in 96-well polystyrene microplates (Greiner Bio-One). Each resuspension was inoculated into four media (Table S2) in triplicate. The plate was covered with optical film, with a small (∼0.5 mm) hole poked above each well, outside of the plate reader's light path, to allow gas exchange.

Incubation and optical density (OD) measurements were performed with an Epoch 2 plate reader (BioTek) in an anaerobic chamber at 37 °C with continuous shaking and OD_{600} measured at 7.5-min intervals. Since some commensals require >24 h to reach saturation (Tramontano et al., 2018), plates were incubated in the plate reader for 48 h and then 1 μL of this saturated culture was transferred into 200 μL of fresh medium in a new plate. We refer to a 48-h cycle from inoculation to saturation as one passage. Samples used in the passaging experiments in Figure 3 were sometimes taken in consecutive days, hence the plate was removed from the plate reader every 24 h, to inoculate and/or passage corresponding SICs. On a given day, if the communities were not passaged, then the whole volume was transferred into a new plate.

After passaging, 50 μL of the cultures were mixed with 50 μL of sterile 50% glycerol (v/v in water) in crimp vials, sealed, and stored at -80 °C for long-term storage. The remaining volume was stored in the 96-well plate at -80 °C with an aluminum seal until DNA was extracted. BHI SICs were revived for experimentation by inoculation of frozen glycerol stocks directly into 3 mL of BHI. Revived communities were incubated at 37 °C for 48 h and passaged twice before experimentation by diluting 1:200 into fresh medium every 48 h.

SIC colonization
Mice were humanized with a human fecal sample obtained from the same healthy anonymous donor as was used for the ciprofloxacin-treatment experiment (Figure 1A). Four weeks after humanization, fecal pellets were collected from 11 mice housed across 3 cages. A mixture of the 11 fecal pellets was used to inoculate 3 mL of BHI to derive an SIC as described above. The SIC was passaged every 48 h with a 1:200 dilution into fresh medium. After 5 passages, a frozen stock was made by mixing equal volumes of a saturated culture and 50% glycerol (v/v in water). The SIC was revived by inoculating the frozen stock into 3 mL of BHI and passaging twice before using 200 μL of the saturated culture to gavage three co-housed germ-free, female, Swiss-Webster mice. Fecal pellets were sampled from the germ-free mice on the day that they were gavaged, on day 24 after colonization for proteome analysis, and on day 28 for 16S sequencing.

Strains and growth media
Growth media are listed in Table S2. These media were chosen because of their ability to grow diverse microbes: the nutrient-rich Brain Heart Infusion (BHI) is widely used to culture fastidious microorganisms; Tryptone-Yeast extract-Glucose (TYG), which is often used to culture members of the *Bacteroides* genus that includes many prevalent human commensals (Whitaker et al., 2017); Gifu Anaerobic Medium (GAM; a mixture of animal, plant, and yeast digests and extracts supplemented with glucose and starch), which cultures individual species with relative yields similar to their abundances in human microbiotas (Rettedal et al., 2014); and Yeast extract, Casitone, and Fatty Acids (YCFA), which has been used to culture a wide range of human gut commensals (Browne et al., 2016). Isolated strains are listed in Table S1. All media and materials were made anaerobic by incubating in a custom anerobic chamber (Coy Labs) for 48 h before use.

16S rRNA gene sequencing
DNA was extracted from whole fecal pellets or 50 μL of culture with a DNeasy PowerSoil HTP 96 kit (Qiagen 12955-4). 16S rRNA gene amplicons were generated using Earth Microbiome Project-recommended 515F/806R primer pairs using the 5PRIME HotMasterMix (Quantabio 2200410) with the following program in a thermocycler: 94 °C for 3 min, 35 cycles of [94 °C for 45 s, 50 °C for 60 s, and 72 °C for 90 s], followed by 72 °C for 10 min. PCR products were cleaned, quantified, and pooled using the UltraClean 96 PCR Cleanup kit (Qiagen 12596-4) and Quant-iT dsDNA High Sensitivity Assay kit (Invitrogen Q33120). Samples were sequenced with 250- or 300-bp reads on a MiSeq (Illumina).

Samples were de-multiplexed with Qiime v. 1.9.1 (Caporaso et al., 2010) using the commands "split_libraries_fastq.py –rev_comp_mapping_barcodes –rev_comp_barcode –store_demultiplexed_fastq –max_bad_run_length 999 –min_per_read_length_fraction.01 –sequence_max_n 999 –phred_quality_threshold 0" and "split_sequence_file_on_sample_ids.py". Subsequent processing was performed using DADA2 as previously described (Callahan et al., 2016). truncLenF and truncLenR parameters were set to 240 and 180, respectively. Resulting ASV sequences were assigned taxonomy with Qiime, using the commands "assign_taxonomy.py", "align_seqs.py", and "make_philogeny.py".

Isolation of strains
SICs were resuspended in PBS and plated onto BHI, BHI-S, or GAM plates. Plates were incubated at 37 °C in an anaerobic chamber. After 2 days, colonies were grown in the medium corresponding to the plate from which they were isolated for 2 days, and glycerol stocked. Strains were identified via high-throughput MALDI-TOF mass spectrometry of whole colonies, and subsequent matching of spectra to a reference library with a MALDI Biotyper System (Bruker), following manufacturer's instructions and including formic acid lysis. Fifteen distinct strains were obtained and their taxonomy was checked by Sanger sequencing. Genomic DNA was extracted from pure cultures using a DNeasy UltraClean 96 Microbial kit (Qiagen 10196-4) or DNeasy Blood and Tissue kit (Qiagen 69504). The

16S gene was amplified using primers 5'AGAGTTTGATCCTGGCTCAG and 5'GACGGGCGGTGWGTRCA, and the amplicon was Sanger sequenced. Taxonomic assignment was performed by alignment using BLAST against the 16S ribosomal RNA sequences (Bacterial and Archaea) database.

Antibiotic sensitivity estimation

Frozen stocks of isolated strains (Table S1) were streaked onto BHI + 5% sheep blood agar plates and incubated for 48 h at 37 °C in anaerobic conditions. A single colony of each strain was inoculated as a monoculture in 3 mL of BHI, and incubated for 48 h at 37 °C. Cultures were then diluted 1:200 into fresh BHI containing 0.5-32 μg/mL ciprofloxacin. The minimum inhibitory concentration (MIC) for each strain was calculated as the minimum dose necessary to completely inhibit growth as measured by OD_{600} after 48 h of incubation.

In vitro Salmonella Typhimurium challenge

SICs were revived in 200 μL BHI in microplates and passaged twice by diluting 1 μL into 200 μL of fresh medium every 48 h. A frozen stock of S. Typhimurium SL1344 was grown anaerobically at 37 °C for 24 h in BHI. One microliter of the SICs and 1 μL of S. Typhimurium adjusted to OD_{600}=0.1 was diluted into 200 μL of fresh BHI. Saturated co-cultures were serially diluted into sterile PBS after 48 h of incubation at 37 °C. Three microliters of a 1:10^4 dilution were spotted onto LB agar with 50 μg/mL streptomycin to select for S. Typhimurium. Pictures of colonies (Figures 4B and S8A) were taken after 48 h of incubation at 37 °C in aerobic conditions.

For single-cell quantification of S. Typhimurium levels, we followed the protocol described above to grow SICs and an S. Typhimurium 14028s strain expressing cytoplasmic mCherry (Table S1) prior to co-culturing. SICs and S. Typhimurium were mixed at various ratios and incubated anaerobically for 48 h at 37 °C. Saturated cultures were removed from the anaerobic chamber and spotted onto PBS agar plates to perform high-throughput phase and fluorescence microscopy (Shi et al., 2017).

In vitro antibiotic treatment

SICs were revived in 3 mL of BHI and passaged twice before experimentation by diluting 15 μL into 3 mL of fresh medium every 48 h. One microliter of the SICs was then diluted into 200 μL of fresh BHI containing 0.5-32 μg/mL ciprofloxacin. Growth was measured in a plate reader as described above, and 48 h-old cultures were stored at -80 °C until DNA was extracted.

Isolation of stool proteins and peptides

Isolation of stool proteins broadly followed the protocol in Gonzalez et al., (2020). Briefly, ∼50 mg of mouse pellets or pelleted cells from 1 mL saturated cultures were aliquoted into a 96-well plate along with ∼600 mg of 0.1-mm ceramic beads (Omni International, #27-6006). To each well, 750 μL of lysis buffer (6 M urea, 5% sodium dodecyl sulfate, and 50 mM Tris, pH 8.1) were added and plates were sealed with sealing mats (Omni International, #27-530). Sealed plates were subjected to 10 min of bead beating at 20 Hz using a Qiagen Tissuelyser II. After bead beating, each plate was centrifuged at 3000 rcf at 4 °C for 10 min. Five hundred microliters of the resulting supernatant were transferred to a new 2-mL 96-well plate (Waters, 186002482), sealed with a sealing mat, spun again at 3000 rcf at 4 °C for 10 min, then transferred to a fresh 2-mL plate. Samples were reduced with 10 μL of 500 mM dithiothreitol (Sigma-Aldrich) for 30 min at 47 °C and alkylated with 30 μL of 500 mM iodoacetamide (Sigma-Aldrich) for 1 h at room temperature in the dark. Fifty microliters of the reduced and alkylated supernatant were transferred to a new 2-mL 96-well plate for further processing, while the remaining material was stored at -80 °C.

Supernatant-resident stool proteins were washed, digested, and eluted as described in the Protifi S-trap protocol (http://www.protifi.com/wp-content/uploads/2018/08/S-Trap-96-well-plate-long-1.4.pdf). Briefly, the 50 μL of supernatant were acidified with 5 μL of 12% phosphoric acid to which 300 μL of S-trap binding buffer was added. Each resulting mixture was loaded into a single well. Positive pressure was used to load the proteins into each well with a Positive Pressure-96 Processor (Waters) with pressure set at 6-9 psi on the "Low-Flow" setting. Loaded proteins were washed with 300 μL of Binding Buffer (90% methanol and 10% triethylammonium bicarbonate buffer (TEAB, Sigma-Aldrich, #T7408), adjusted to pH 7.1 using phosphoric acid) five times. After washing, 125 μL of digestion buffer (100 mM TEAB and 5 μg trypsin) were added and proteins were digested for 3 h at 47 °C. Peptides were eluted with 100 μL of TEAB, followed by 100 μL of 0.2% formic acid, followed by 100 μL of 50% acetonitrile, 0.2% formic acid. These peptides were captured in a 1-mL 96-well plate (Thermo Scientific, #AB-1127) and the volume was dried down in a Centrivap speedvac (Model 7810016). Plated samples were desalted using RP-S cartridges on an Agilent Bravo AssayMAP using the built-in desalting protocol, eluted with 50% acetontrile, and dried down. Plated peptide concentrations were normalized using a Nanodrop ND-1000.

Mass spectrometry

Peptide samples were diluted to 0.5 μg/μL. Subsequently, 1 μL was loaded onto an in-house, laser-pulled 100-μm inner diameter nanospray column packed to ∼220 mm with 3-μm 2A C18 beads (Reprosil). Peptides were separated by reversed-phase chromatography on a Dionex Ultimate 3000 HPLC. Buffer A of the mobile phase contained 0.1% formic acid in HPLC-grade water, and buffer B contained 0.1% formic acid in acetonitrile. An initial 2-min isocratic gradient flowing 3% B was followed by a linear increase to 25% B for 115 min, then increased to 45% B over 15 min, and a final increase to 95% B over 15 min, whereupon B was held for 6 min and returned back to baseline in 2 min and held for 10 min, for a total of 183 min. The HPLC flow rate was 0.400 μL/min. Samples were run on a Thermo Fusion Lumos mass spectrometer that collected mass spectrometry data in positive-ion mode within the 400-1500 (Bar-

thel et al., 2003; Lozupone and Knight, 2005) *m/z* range with an initial Orbitrap scan resolution of 120,000, followed by high-energy collision-induced dissociation and analysis in the orbitrap using "Top Speed" dynamic identification with dynamic exclusion enabled (repeat count of 1, exclusion duration of 90 s). The automatic gain control was set to 4×10^5 for FT full mass spectrometry and to 10^4 for ITMSn.

Peptide/protein database searching

Mass spectra were searched using Proteome Discoverer 2.2 using the built-in SEQUEST search algorithm. Two FASTA databases were searched: Uniprot Swiss-Prot *Mus musculus* (taxon ID 10090, downloaded January 2017) and a database containing common preparatory contaminants. Target-decoy searching at both the peptide and protein level was employed with a strict false discovery-rate cutoff of 0.05 using the Percolator algorithm built into Proteome Discoverer 2.2. Enzyme specificity was set to tryptic, with static peptide modifications set to cambamidomethylation (+57.0214 Da). Dynamic modifications were set to oxidation (+15.995 Da) and N-terminal protein acetylation (+42.011 Da). Only high-confidence proteins ($q < 0.01$) were used for analysis.

QUANTIFICATION AND STATISTICAL ANALYSIS

16S data analysis

Custom MATLAB (MathWorks) scripts were used for 16S data analysis.

ASVs were classified as contaminants and removed from further analysis if they appeared with significantly higher relative abundances ($p<0.001$, t-test) in control samples (water added to DNA extraction step).

Alpha diversity (richness) was measured by rarefying all samples to 5000 reads and calculating the number of taxa with relative abundance >0. Shannon diversity was calculated using $S = \sum_{i=1}^{N} (- p_i \ln p_i)$, where p_i is the relative abundance of the *i*th taxon and *N* is the total number of taxa with $p_i>0$. Evenness was calculated using the Pielou index by normalizing Shannon diversity by the maximum Shannon index for the number of taxa: $J = S/\ln N$.

Weighted and unweighted Unifrac distances between samples were calculated using custom MATLAB code. Unifrac was calculated as described in Lozupone and Knight, (2005). Weighted Unifrac was calculated as described in Lozupone et al., (2007): for samples *A* and *B*, $u_w = \sum_{i}^{n} b_i \times |A_i - B_i|$, where *n* is the total number of branches in the tree, b_i is the length of branch *i*, and A_i and B_i are the relative abundances of the taxa that descend from branch *i* in samples *A* and *B*, respectively. No further normalization was performed. Only taxa present at >0.01% in more than two samples were used to calculate distances. Principal coordinate analyses were performed on unweighted Unifrac distances between samples with >5000 reads.

Growth analyses

Maximal growth rate was calculated as the maximal slope of ln(OD) with respect to time (calculated from a linear regression of a sliding window of 11 timepoints) using custom Matlab (Mathworks) code.

Proteome analysis

Custom MATLAB R2018a (MathWorks) scripts were used to analyze protein abundances. *M. musculus* analyses were restricted to proteins that were 10 times more abundant in germ-free, humanized, or SIC-colonized mice samples than in any *in vitro* bacterial cultures in our dataset.

Bacterial invasion

Percentages of *S*. Typhimurium (Figures 4C and S7B) were estimated by calculating the proportion of pixels within cell contours segmented from phase images whose fluorescence was above a threshold that clearly separated mCherry-positive and mCherry-negative cells using custom Matlab code.

Statistical analyses

For two-condition comparisons, two-sample t-tests were applied. Pearson correlation coefficients and the *p*-values for testing the hypothesis that there is no relationship between the observed phenomena were calculated on $\log_{10}$(relative abundance).